JPE 9-4-8

Wide Speed Direct Torque and Flux Controlled IPM Synchronous Motor Drive Using a Combined Adaptive Sliding Mode Observer and HF Signal Injection

Gilbert Foo[†] and M. F. Rahman[*]

[†*]School of Electrical Eng. and Telecommunications, The University of New South Wales, Sydney, Australia

ABSTRACT

This paper proposes a new speed sensorless direct torque and flux controlled interior permanent magnet synchronous motor (IPMSM) drive. Closed-loop control of both the torque and stator flux linkage are achieved by using two proportional-integral (PI) controllers. The reference voltage vectors are generated by a SVM unit. The drive uses an adaptive sliding mode observer for joint stator flux and rotor speed estimation. Global asymptotic stability of the observer is achieved via Lyapunov analysis. At low speeds, the observer is combined with the high frequency signal injection technique for stable operation down to standstill. Hence, the sensorless drive is capable of exhibiting high dynamic and steady-state performances over a wide speed range. The operating range of the direct torque and flux controlled (DTFC) drive is extended into the high speed region by incorporating field weakening. Experimental results confirm the effectiveness of the proposed method.

Keywords: Adaptive sliding mode observer, Direct torque and flux control, Sensorless, Signal injection, Zero speed

1. Introduction

Interior permanent magnet synchronous motors (IPMSMs) are receiving increased attention in recent years because of their high efficiency, large torque to volume ratio and reliable operation. In many drive applications, field oriented control (FOC) or vector control is used. In the late 1990's, the DTC was successfully implemented on interior permanent magnet synchronous motors (IPMSMs)[3-6]. The block diagram of the classical DTC is depicted in fig. 1. When compared to conventional vector controlled drives, DTC possesses several advantages such as elimination of coordinate transformation, less parameter dependence and faster dynamic response[7]. As the torque and flux are regulated directly and independently, DTC features fast responses. Furthermore, due to the absence of coordinate transformation, DTC is inherently sensorless. Nevertheless, the inability to accurately estimate the stator flux at low speeds is its main drawbacks. As a result, sensorless operation at low speeds is a problem common to both the DTC and the FOC. Usage of an encoder for stable operation at low speeds seems to negate the benefits of the DTC. In addition, the presence of a position sensor

Manuscript received December 19, 2008; revised May 11, 2009
[†]Corresponding Author: gilbert.foo@student.unsw.edu.au
Tel: +61-2-9385-5904, Fax: +61-2-9385-5993, UNSW
[*]Dept. of Electrical Eng. and Telecommunications, UNSW, Australia

increases the cost while reducing the reliability of the system.

Several algorithms have been suggested in recent literature to achieve sensorless operation. Back-emf based estimators with explicit compensation for nonlinear properties, parameter variation and disturbances have been proposed[5-7, 12-13]. The open-loop estimator of the traditional DTC falls into this category. This method works reasonably well at high speeds but at low speeds, its performance deteriorates drastically due to the fact that the back-emf being too small to be detected.

Estimation based on high frequency signal injection, exploiting the saliency property of an IPMSM have been reported[10, 14-16]. High frequency signal injection offers a solution at standstill and low speeds but as the speed increases, its performance deteriorates drastically. Furthermore, it may require accurate and precise measurements of the machine parameters.

Since this is not possible, the third form of observer is sometimes more favorable due to its robustness to parameter variations and its excellent disturbance rejection capabilities. The Extended Kalman Filter (EKF) approach has been suggested[11,19-20]. The EKF can give recursive optimum state estimation for IPM machines using terminal signals that may be polluted by noise but is highly computational extensive because it involves vector and matrix operations. Furthermore, extreme care has to be exercised in selecting the noise covariance matrices and initial values for the algorithm to avoid instability. Until now, there is no clear approach to choosing these matrices.

The application of an adaptive sliding observer for direct torque controlled IPM synchronous motor drives has been reported[17, 18]. In this approach, stable operation at 10 rpm with half-full load was achieved. But, it is worth noting that this was achieved with a reduction in inverter gain. In addition, the model is very complicated due to the inclusion of the extended electromotive forces (EEMFs) as state variables.

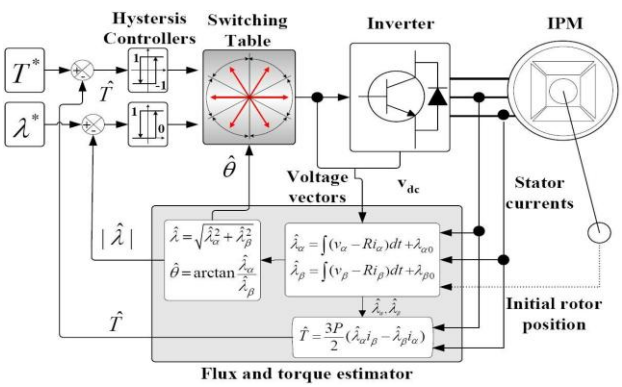

Fig. 1. Block diagram of the classical DTC.

In this paper, a sliding mode observer in the rotating *(d-q)* reference frame for joint stator flux and rotor speed estimation is proposed. Sliding mode observers present several benefits such as high state estimation accuracy, excellent dynamic properties, robustness to parameter variations and their ability to handle nonlinear systems like the IPMSM very well. The stability of this observer can be determined via Lyapunov stability analysis. At low speeds, the high frequency signal injection approach is used in conjunction with the observer to enable stable operation down to zero speed. The estimated torque and flux linkage are then regulated via the direct torque and flux control (DTFC) approach[16]. This method uses the space vector modulation (SVM) technique and hence, it suppresses the torque and flux ripples significantly.

This paper is organized as follows. Firstly, the SVM-DTFC technique is highlighted. Next, an elaborate presentation of the adaptive sliding mode observer followed by a brief review of the high-frequency signal injection technique is given. Next, the maximum torque per ampere (MTPA) and field weakening (FW) regimes are briefly treated. Finally, experimental results to validate the effectiveness of the proposed sensorless SVM-DTFC drive are presented.

2. SVM-DTFC Scheme

The stator flux linkage vector, λ_s and the rotor flux linkage vector, λ_f can be drawn in the rotor flux (*d-q*), stator flux (*x-y*) and stationary (α-β) frames. The various reference frames are depicted in Fig. 2. The machine equations in the rotor (*d-q)* reference frame are as follows[3]:

$$\begin{cases} v_d = R_s i_d + \dfrac{d\lambda_d}{dt} - \omega_{re}\lambda_q \\ v_q = R_s i_q + \dfrac{d\lambda_q}{dt} + \omega_{re}\lambda_d \end{cases} \quad (1)$$

$$\begin{cases} \lambda_d = L_d i_d + \lambda_f \\ \lambda_q = L_q i_q \end{cases} \tag{2}$$

where L_d , L_q and R_s are the machine dq axes inductances and stator resistance respectively. With (3), these equations can be transformed to the *x-y* reference frame.

$$\begin{pmatrix} F_x \\ F_y \end{pmatrix} = \begin{pmatrix} \cos\delta & \sin\delta \\ -\sin\delta & \cos\delta \end{pmatrix} \begin{pmatrix} F_d \\ F_q \end{pmatrix} \tag{3}$$

Where δ is the load angle and F represents voltage, current or flux linkage. Furthermore, it can be shown that the torque T of an IPMSM in the *x-y* reference frame is given by:

$$T = \frac{3}{2} P |\lambda_s| i_y \tag{4}$$

where P is the number of pole pairs in the machine. From (4), we can deduce that the torque is directly proportional to the *y*-axis component of the stator current if the amplitude of the stator flux linkage is constant. Substituting (1) into (3), we obtain:

$$\begin{cases} v_x = R_s i_x + \dfrac{d\lambda_x}{dt} = R_s i_x + \dfrac{d|\lambda_s|}{dt} \\ v_y = R_s i_y + \omega_s \lambda_x = \dfrac{2R_s}{3P|\lambda_s|} T + \omega_s |\lambda_s| \end{cases} \tag{5}$$

Equation (5) shows that the stator flux can be directly regulated by the *x*-component of the stator voltage. In addition, provided that the amplitude of the stator flux is constant, the *y*-component of the stator voltage is qualified to regulate the torque of the machine.

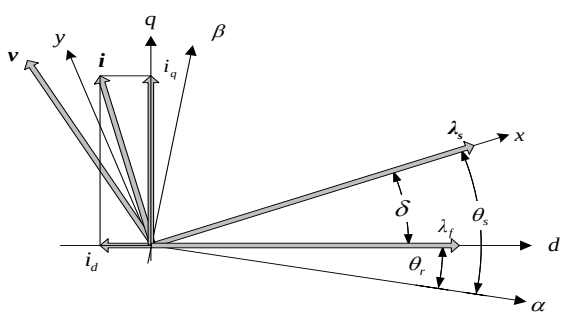

Fig. 2. The stator and rotor flux linkages in various reference frames.

Based on the above analysis, a DTFC method based on SVM for independent torque and flux regulation can be developed. The SVM-DTFC controller consists of two PI regulators – one for flux and one for torque. The inputs of the PI controllers are the torque and flux errors while the outputs are the *x-y* reference voltage vectors. Since PI controllers are present in both the flux and torque channels, the disturbance terms $R_s i_x$ and $\omega_s |\lambda_s|$ in (5) can be ignored. The reference voltage vector should be transformed to the stationary frame via (6) before using the SVM algorithm.

$$\begin{pmatrix} v_\alpha \\ v_\beta \end{pmatrix} = \begin{pmatrix} \cos\theta_s & -\sin\theta_s \\ \sin\theta_s & \cos\theta_s \end{pmatrix} \begin{pmatrix} v_x \\ v_y \end{pmatrix} \tag{6}$$

where θ_s is the stator flux angle and it can be calculated from:

$$\theta_s = \tan^{-1}\left(\frac{\lambda_\beta}{\lambda_\alpha}\right) \tag{7}$$

The stator flux linkage and the torque are estimated using the adaptive sliding mode observer which will be explained next.

3. Adaptive Sliding Mode Observer

3.1 Design of the Observer

Assuming orientation, the stator current i_d, i_q is taken as the output. Based on the machine model in (1) and (2), the structure of the adaptive sliding mode observer can be expressed as:

$$\begin{pmatrix} \dot{\hat{\lambda}}_d \\ \dot{\hat{\lambda}}_q \end{pmatrix} = \begin{pmatrix} -\dfrac{\hat{R}_s}{L_d} & \hat{\omega}_{re} \\ -\hat{\omega}_{re} & -\dfrac{\hat{R}_s}{L_q} \end{pmatrix} \begin{pmatrix} \hat{\lambda}_d \\ \hat{\lambda}_q \end{pmatrix} + \begin{pmatrix} v_d \\ v_q \end{pmatrix} + \begin{pmatrix} \dfrac{\hat{R}_s}{L_d}\lambda_f \\ 0 \end{pmatrix} + KS + \Phi sign(S)$$

$$\begin{pmatrix} i_d \\ i_q \end{pmatrix} = \begin{pmatrix} \dfrac{1}{L_d} & 0 \\ 0 & \dfrac{1}{L_q} \end{pmatrix} \begin{pmatrix} \hat{\lambda}_d \\ \hat{\lambda}_q \end{pmatrix} - \begin{pmatrix} \dfrac{\lambda_f}{L_d} \\ 0 \end{pmatrix} \tag{8}$$

where ^ denotes estimated quantities and K and Φ are gains of the observer. The observer uses both linear K and nonlinear Φ feedback terms. The linear feedback

gain is responsible for the desired closed loop error dynamics while the nonlinear gain ensures the robustness of the observer. The sliding hyperplane is defined upon the stator current errors.

$$S=\begin{pmatrix}S_1\\S_2\end{pmatrix}=\begin{pmatrix}i_d-\hat{i}_d\\i_q-\hat{i}_q\end{pmatrix}=0 \tag{9}$$

3.2 Lyapunov stability analysis

The state estimation error dynamics is given by:

$$\dot{\tilde{x}}=\frac{d}{dt}\begin{pmatrix}\lambda_d-\hat{\lambda}_d\\\lambda_q-\hat{\lambda}_q\end{pmatrix}$$

$$=(A-KC)\tilde{x}+\tilde{\omega}_{re}\begin{pmatrix}\hat{\lambda}_q\\-\hat{\lambda}_d\end{pmatrix}+\tilde{R}_s\begin{pmatrix}-\frac{1}{L_d}\hat{\lambda}_d+\frac{\lambda_f}{L_d}\\-\frac{1}{L_q}\hat{\lambda}_q\end{pmatrix}-\Phi sign(S) \tag{10}$$

where:

$$A=\begin{pmatrix}-\frac{R_s}{L_d} & \omega_{re}\\-\omega_{re} & -\frac{R_s}{L_q}\end{pmatrix},C=\begin{pmatrix}\frac{1}{L_d} & 0\\0 & \frac{1}{L_q}\end{pmatrix},\tilde{\omega}_{re}=\omega_{re}-\hat{\omega}_{re},\tilde{R}_s=R_s-\hat{R}_s.$$

In order to determine the stability of the designated observer, let the Lyapunov function be:

$$V=\frac{1}{2}(\tilde{x}^T\tilde{x}+\frac{\tilde{\omega}_{re}{}^2}{\gamma_1}+\frac{\tilde{R}_s^2}{\gamma_2}) \tag{11}$$

where $\gamma_1,\gamma_2>0$. Assuming that the rotor angular velocity and stator resistance are constant within a sampling interval,

$$\dot{V}=\tilde{x}^T\dot{\tilde{x}}-\frac{\dot{\hat{\omega}}_{re}}{\gamma_1}\tilde{\omega}_{re}-\frac{\dot{\hat{R}}_s}{\gamma_2}\tilde{R}_s \tag{12}$$

substituting (10) into (12) yields:

$$\dot{V}=\tilde{x}^T(A-KC)\tilde{x}-\tilde{\omega}_{re}[\hat{\lambda}_q\tilde{\lambda}_d-\hat{\lambda}_d\tilde{\lambda}_q-\frac{\dot{\hat{\omega}}_{re}}{\gamma_1}]-\hat{R}_s[-\tilde{\lambda}_d\hat{i}_d-\tilde{\lambda}_q\hat{i}_q$$

$$-\frac{\dot{\hat{R}}_s}{\gamma_2}]-S^T\Phi sign(S)$$

$$=S^TC^{-1}(A-KC)CS-\tilde{\omega}_{re}[\hat{\lambda}_q\tilde{\lambda}_d-\hat{\lambda}_d\tilde{\lambda}_q-\frac{\dot{\hat{\omega}}_{re}}{\gamma_1}]-\hat{R}_s[-\tilde{\lambda}_d\hat{i}_d$$

$$-\tilde{\lambda}_q\hat{i}_q-\frac{\dot{\hat{R}}_s}{\gamma_2}]-\tilde{x}^T\Phi sign(\tilde{x}) \tag{13}$$

For global asymptotic stability, $\dot{V}<0$. Thus, the following equations are obtained:

$$(A-KC)<0 \tag{14}$$

$$\hat{\lambda}_q\tilde{\lambda}_d-\hat{\lambda}_d\tilde{\lambda}_q-\frac{\dot{\hat{\omega}}_{re}}{\gamma_1}=0 \tag{15}$$

$$-\tilde{\lambda}_d\hat{i}_d-\tilde{\lambda}_q\hat{i}_q-\frac{\dot{\hat{R}}_s}{\gamma_2}=0 \tag{16}$$

$$\tilde{x}^T\Phi sign(\tilde{x})>0 \tag{17}$$

From (14), the eigenvalues of $(A-KC)$ are required to be in the left-half plane. Hence, the gain K can be found by pole placement. Furthermore, if $\Phi=\begin{pmatrix}\Phi_{11} & 0\\0 & \Phi_{22}\end{pmatrix}$, from (17), then $\Phi_{11},\Phi_{22}>0$. Larger values of Φ_{11},Φ_{22} increase the robustness of the observer but may generate unwanted chattering.

From (18) and (19), the following update laws for rotor speed and stator resistance estimation can be deduced:

$$\hat{\omega}_{re}=\gamma_1\int(\hat{\lambda}_q\tilde{\lambda}_d-\hat{\lambda}_d\tilde{\lambda}_q)dt \tag{18}$$

$$\hat{R}_s=-\gamma_2\int(\tilde{\lambda}_d\hat{i}_d+\tilde{\lambda}_q\hat{i}_q)dt \tag{19}$$

4. FVD and Dead-time Compensation

Voltage drops across power switches in the inverter reduce the terminal voltage seen by the machine. At very low speeds, the voltage drop can be higher than the induced voltage and hence introduce a severe disturbance. It is shown that the error voltage vector of the three inverter legs can be represented by[25]:

$$V_{fvd}=\frac{2}{3}v_{CE}[\mathrm{sgn}(i_A)+\alpha*\mathrm{sgn}(i_B)+\alpha^2*\mathrm{sgn}(i_C)] \tag{20}$$

where $\alpha = e^{j2\pi/3}$ and v_{CE} is the forward voltage drop of the switch. From (20), it is seen that the voltage error vector only depends on the polarity of the three-phase currents. Hence, for the purpose of compensating the error vector, only the polarities of the three phase currents are needed.

There is a time in each switching cycle where both the high and low side switches in the same leg of the inverter are off and the current flow is through the diodes. This is known as dead-time which is inserted into the gate signal of the switch that is to be turned on to avoid a direct short circuit across the DC bus voltage source. This dead-time delay causes a change in and distortion of the stator voltage vector applied to the machine.

Fig. 3 shows the PWM control signal as an example and the switching signals of a single inverter leg. The control signals for the upper and lower switches are shown together with the dead-time. The turn-on and turn-off time of the power switches are also considered in the figure. In the last two subplots of Fig. 3, the expected and the actual output voltages are compared. It is seen that due to the effect of dead-time t_d, the turn-on delay t_{ON} and the turn-off delay t_{OFF}, there is distortion between the expected and the actual output voltages.

The dead-time error vector between the expected output and the actual voltage vector is given by (21) for different directions of the current vector. This error can be compensated for by detecting the polarity of the output current.

$$V_{dt} = \frac{2}{3} V_{dead} [\mathrm{sgn}(i_a) + \alpha * \mathrm{sgn}(i_b) + \alpha^2 \mathrm{sgn}(i_c)] \quad (21)$$

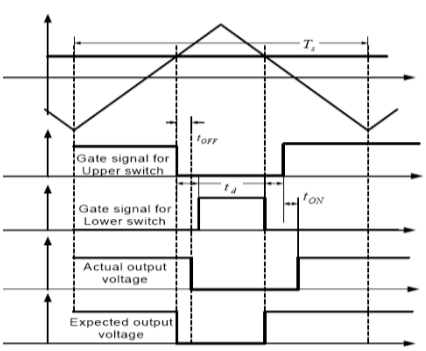

Fig. 3. PWM switching signals of the inverter with positive current considering the effect of dead-time and switching delays in the power switches.

where: $V_{dead} = V_{dc}\left(\frac{t_d + t_{on} - t_{off}}{T_s}\right)$ (22)

where V_{dc} and T_s are the dc-link voltage and switching periods respectively. The compensation in (22) must be made to the reference voltage vector V_{ref} which is used by the observer as the input $V_{\alpha,\beta}$ for more accurate observation.

$$V_{\alpha,\beta} = V_{ref} - (V_{fvd} + V_{dt}) = V_{ref} - \Delta V \quad (23)$$

5. HF Signal Injection

At very low speeds, the stator voltage becomes very small and the effects of inverter nonlinearities become severe. This can easily lead the drive system to instability. To solve this problem, the high frequency (HF) signal injection method can be combined with the proposed sliding mode observer. Several HF injection methods can be found in the literature. These methods can be classified into *α-β* reference frame rotating injection[21], *d-q* reference frame pulsating injection[22] and *d-q* reference frame rotating injection[23]. In this paper, the *d-q* reference frame persistent HF rotating carrier injection is implemented, where an alternating voltage is used for injection. A carrier excitation signal fluctuating at angular frequency ω_c, and having amplitude V_c, as shown in (24), is superimposed on the d- component of the stator voltage in the estimated rotor reference frame.

$$V_{hf} = V_c \cos(\omega_c t) \quad (24)$$

The frequency of the injected voltage carrier, ω_c, should be high enough to ensure sufficient spectral separation between itself and the fundamental excitation to reduce the requirements of the band-pass filters. An alternating HF current response is detected in the q direction of the estimated rotor reference frame with its amplitude modulated by the rotor position estimation error. The method of the demodulation process is shown in Fig. 4. The high frequency component of the measured current in the q-direction, i_{qc}, is obtained by band-pass filtering (BPF) of the *q* component of the measured current. The HF current signal is then demodulated and low-pass

filtered (LPF) to extract an error signal given by:

$$\varepsilon = LPF\{i_{qc}\sin(\omega_c t)\} \tag{25}$$

This error signal is ideally[15]:

$$\varepsilon = K_\varepsilon \sin(\tilde{\theta}_m) \tag{26}$$

Assuming the estimated error is small, (26) can be approximated by:

$$\varepsilon = 2K_\varepsilon \tilde{\theta}_m \tag{27}$$

The error signal is used for correction of the estimated rotor position by augmenting the sliding mode observer as follows:

$$\begin{pmatrix}\dot{\hat{\lambda}}_d\\ \dot{\hat{\lambda}}_q\end{pmatrix} = \begin{pmatrix}-\frac{\hat{R}_s}{L_d} & (\hat{\omega}_{re}+\omega_\varepsilon)\\ -(\hat{\omega}_{re}+\omega_\varepsilon) & -\frac{\hat{R}_s}{L_q}\end{pmatrix}\begin{pmatrix}\hat{\lambda}_d\\ \hat{\lambda}_q\end{pmatrix} + \begin{pmatrix}v_d\\ v_q\end{pmatrix} + \begin{pmatrix}\frac{\hat{R}_s}{L_d}\lambda_f\\ 0\end{pmatrix} + KS + \Phi sign(S)$$

$$\begin{pmatrix}i_d\\ i_q\end{pmatrix} = \begin{pmatrix}\frac{1}{L_d} & 0\\ 0 & \frac{1}{L_q}\end{pmatrix}\begin{pmatrix}\hat{\lambda}_d\\ \hat{\lambda}_q\end{pmatrix} - \begin{pmatrix}\frac{\lambda_f}{L_d}\\ 0\end{pmatrix} \tag{28}$$

where: $$\omega_\varepsilon = K_p\varepsilon + K_i\int \varepsilon dt \tag{29}$$

In this configuration, the signal injection method persists in a steady-state while the sliding mode observer dominates during transients. To ensure a smooth transition between the low and high speed regions, the amplitude of the injected signal, V_c and the PI controller gains, K_p and K_i are decreased linearly with increasing speed, i.e.:

$$\begin{cases}V_c = V_{c0} f(\hat{\omega}_{re})\\ K_p = K_{p0} f(\hat{\omega}_{re})\\ K_i = K_{i0} f(\hat{\omega}_{re})\end{cases} \tag{30}$$

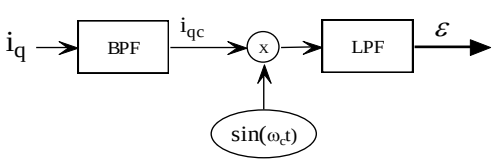

Fig. 4. Demodulation scheme used to obtain error signal.

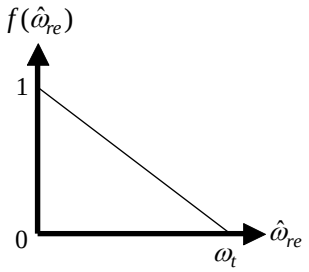

Fig. 5. Speed-dependant function $f(\hat{\omega}_{re})$.

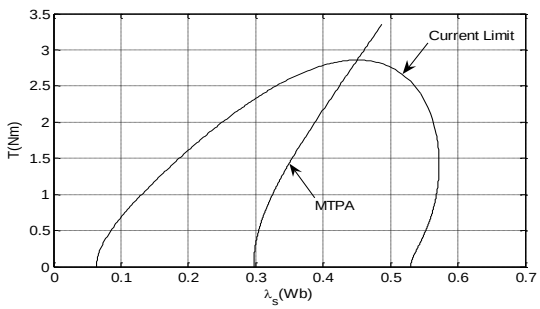

Fig. 6. T-λ_s plane of an IPM machine.

6. Trajectory Control for the DTFC IPM Motor Drive

One prominent advantage of an IPM motor is its wide constant power region or high flux weakening capability. In a DTFC drive, the operation area on the $T-\lambda_s$ plane is restricted by a current limit and voltage limit trajectories at different speeds. The $T-\lambda_s$ plane of a typical IPM machine is illustrated in fig. 6.

In order to achieve high efficiency, the maximum torque per ampere (MTPA) control is adopted for an IPM motor below base speed. For operation above the crossover speed, field weakening control[24] is selected since the voltage would go beyond its limit if the torque and stator flux linkage were still controlled along the MTPA trajectory. If the rotor speed is between the base speed ω_b and crossover speed ω_c, the torque determines the control action. If the voltage requirement of the actual torque exceeds its limit, the control action switches to flux weakening mode. Otherwise, constant torque operation is selected although the rotor speed is above the base speed. Fig. 7 depicts the flow chart for switching between the two control modes[4].

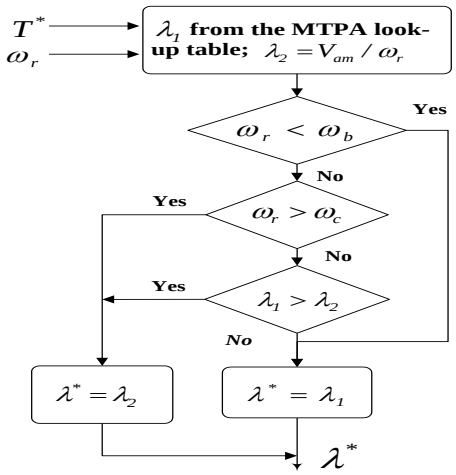

Fig. 7. Determination of the reference stator flux linkage at different speeds.

6. Experimental Results

The effectiveness of the proposed sensorless drive scheme was tested experimentally. The block diagram of the sensorless drive is shown in fig. 8. A DS1104 DSP card was used to carry out the real-time algorithm. A three-phase insulated gate bipolar transistor (IGBT) intelligent power-module is used for an inverter. Coding of real-time control software was done using C language. The PWM signals were generated on the DS1104 board. In experiments, the sampling period of the drive was set to 200μs. A dc machine whose armature current is separately regulated is used to emulate the load. The IPM machine (IPM I) whose parameters are tabulated in table 1 was used in the experiments. An incremental encoder was used to obtain the position signal which was used solely for comparison and not for control purposes. The reference flux value was selected according to the maximum torque per ampere (MTPA) trajectory to increase the efficiency of the overall drive system.

Table 1. Parameters of IPMSM used in this paper.

		IPM I	IPM II
Number of poles	P	4	4
Stator resistance	R_s	5.8 Ω	5.5 Ω
Magnet flux linkage	λ_f	0.533 Wb	0.297 Wb
d-axis inductance	L_d	0.0447 H	0.0868 H
q-axis inductance	L_q	0.1024 H	0.1697 H
Phase voltage	V	132 V	115 V
Line current	I	3 A	1.9 A
Base speed	ω_b	1500 rpm	1500 rpm
Rated torque	T	6 Nm	2.85 Nm

Sensorless zero speed operation with nominal torque steps is depicted in fig. 9. Hence, the combined signal injection-adaptive sliding mode observer is capable of persistent zero speed operation with a full-load. The load was initially applied to the machine and was subsequently removed. It can be observed that the estimated speed tracks the actual speed very well and that the position estimation error is very small during the transients and steady-state. Hence, the sensorless DTFC drive is capable of persistent zero speed operation with a full-load.

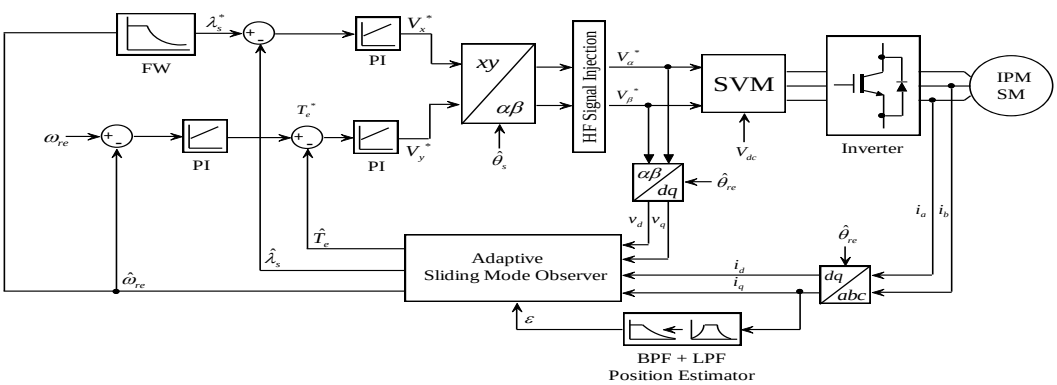

Fig. 8. Block diagram of the sensorless SVM-DTFC scheme.

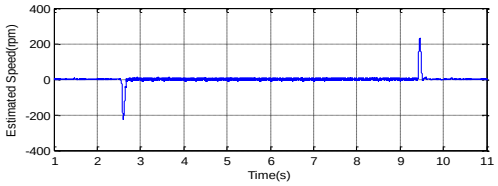

(a) actual speed

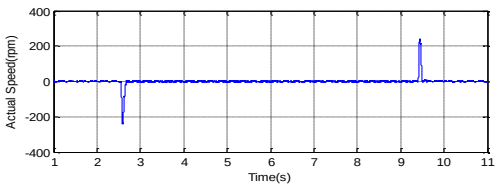

(b) estimated speed

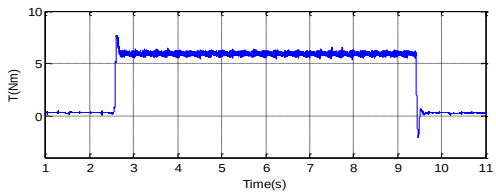

(c) torque

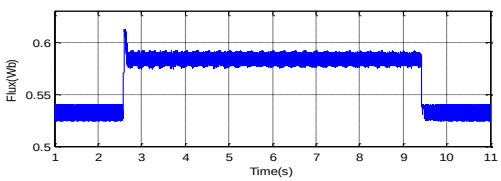

(d) flux

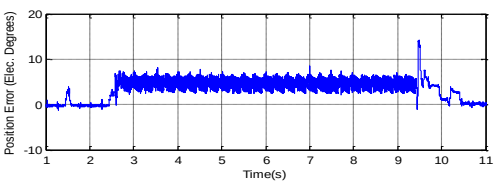

(e) position estimation error

Fig. 9. Full-load steps at standstill.

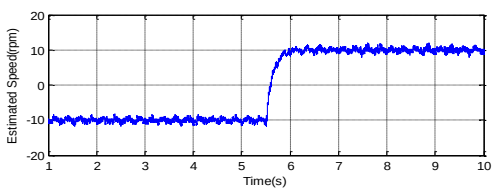

(a) actual speed

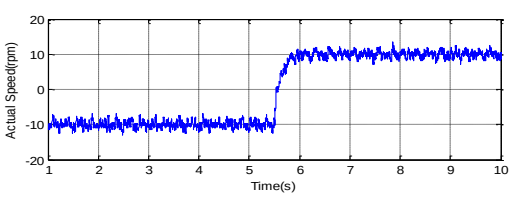

(b) estimated speed

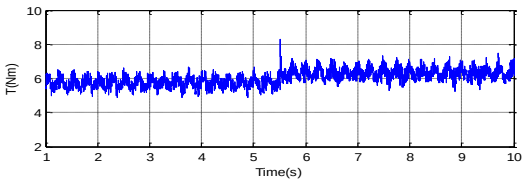

(c) torque

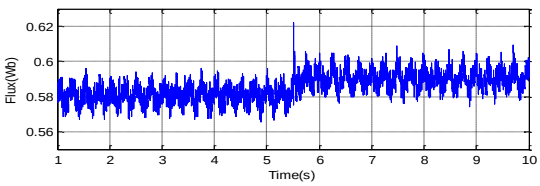

(d) flux

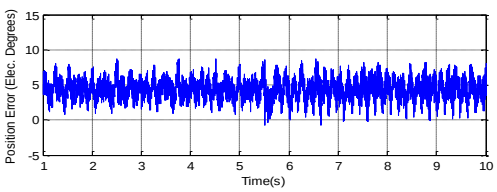

(e) position estimation error

Fig. 10. Full-load speed reversal from -10 rpm to + 10 rpm.

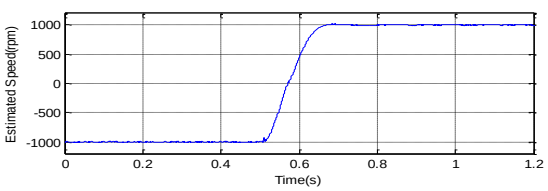

(a) actual speed

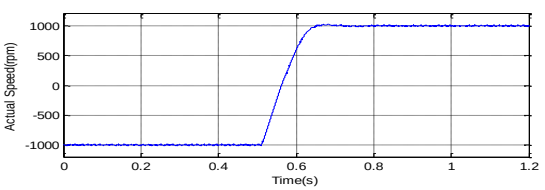

(b) estimated speed

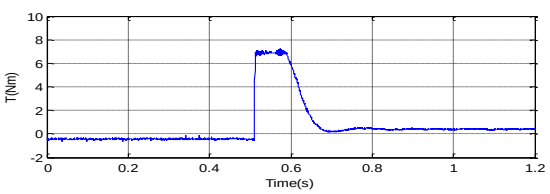

(c) torque

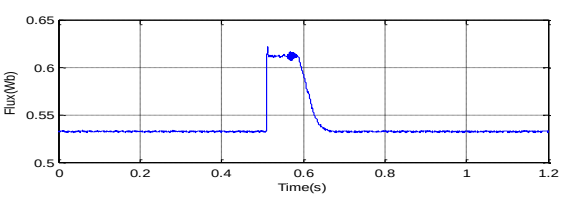

(d) flux

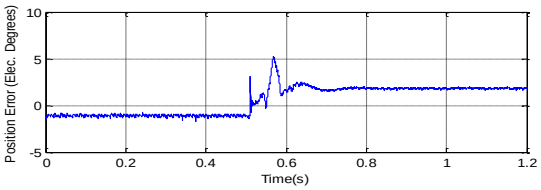

(e) position estimation error

Fig. 11. Speed reversal from -1000 rpm to + 1000 rpm.

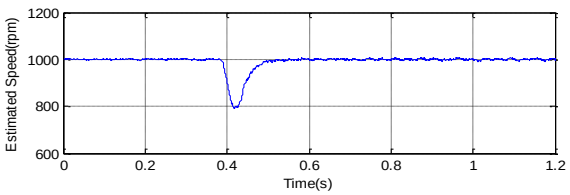

(a) actual speed

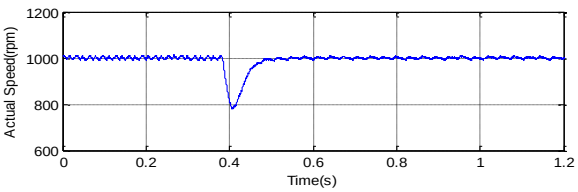

(b) estimated speed

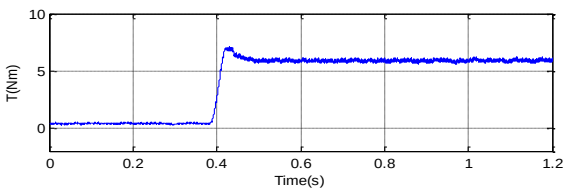

(c) torque

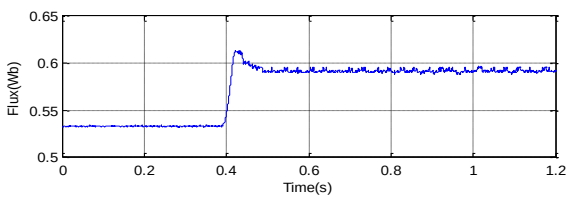

(d) flux

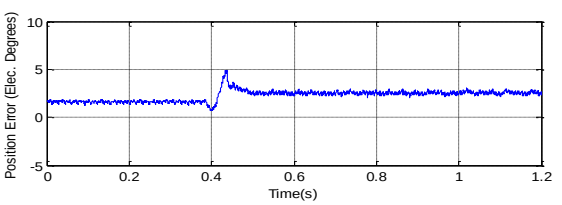

(e) position estimation error

Fig. 12. Full-load step at 1000 rpm.

The low-speed dynamic response of the sensorless drive is shown in fig. 10. The machine is reversed from -5rpm to 5rpm with a full-load. The estimated speed follows the actual speed very well during the reversal, confirming the

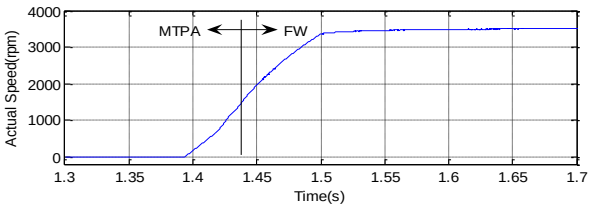

(a) actual speed

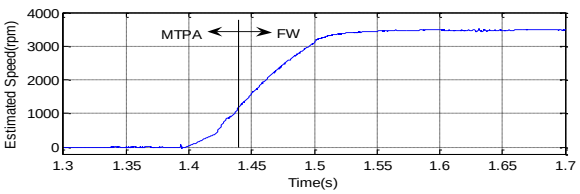

(b) estimated speed

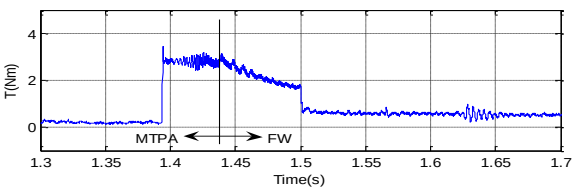

(c) torque

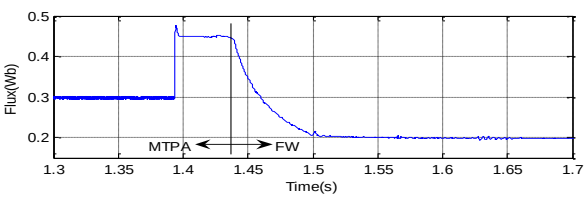

(d) flux

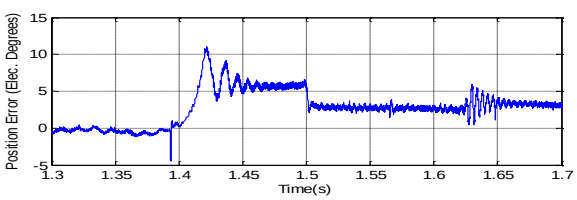

(e) position estimation error

Fig. 13. Field weakening operation from start-up to 3500 rpm.

effectiveness of the combined sliding mode-high frequency signal injection observer.

The dynamic performance of the proposed sensorless drive when the machine is accelerated from -1000 rpm to 1000 rpm is illustrated in fig. 11. There exists a transition from the HF signal injection method to the sliding mode observer. The transition speed is ω_t = 300 rpm. The speed, torque and flux responses in fig. 11 indicate a smooth transition between both observers. Clearly, the estimated

speed tracks the actual speed closely during the transition.

The steady-state performance of the sliding mode observer at 1000 rpm under a full load condition is depicted in fig. 12. The machine was initially running at no-load and nominal torque was abruptly applied to its shaft. From the figures, we can observe that the proposed sliding mode observer is effective even under loaded conditions at high speeds.

To demonstrate the field weakening operation of the sensorless DTFC drive, another IPM machine (IPM II) with flux weakening capability is used. The parameters of IPM machine II is also listed in table 1. IPM machine II has a base and crossover speeds of 1500 rpm and 2400 rpm respectively. Hence, the MTPA trajectory is followed up to 1500 rpm while flux weakening mode is selected for speeds above 1500 rpm. Both the MTPA and FW trajectories are stored in a look-up table to save a considerable amount of computation time.

The field weakening performance of the sensorless DTFC drive can be appreciated from fig. 13. The IPM machine is started-up from rest to its maximum speed of 4000 rpm. The transitions from the signal injection to the sliding mode flux observers and from MTPA to FW modes are smooth with the estimated speed following the actual speed closely during the transition period. The $T-\lambda_s$ characteristics of IPM machine II and the actual torque-flux trajectories are shown in fig. 14. The torque and flux values actually coincide with the MTPA and FW trajectories. Hence, the DTFC drive is able to deliver a high flux weakening performance without a speed sensor.

5. Conclusions

In this paper, a novel adaptive sliding mode flux observer for direct torque and flux control of interior permanent magnet synchronous motor (IPMSM) drives was presented. Global asymptotic stability was achieved via the Lyapunov stability analysis. The proposed observer was combined with the high frequency signal injection method to further enhance the performance of the drive at very low speeds including standstill. Hence, the observer is capable of exhibiting a high steady-state and dynamic performances over a wide range of speeds. Field weakening was integrated into the sensorless scheme to further extend the operating speed region. The proposed method is capable of handling a full-load over the entire speed range. Experimental results demonstrate the effectiveness of the proposed wide speed sensorless DTFC drive.

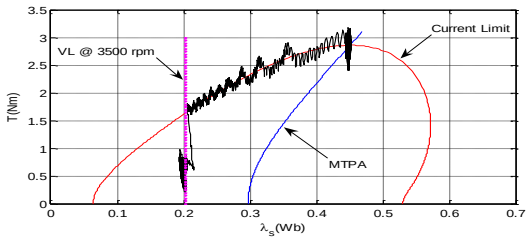

Fig. 14. The $T-\lambda_s$ characteristics of IPM machine II.

References

[1] M. Depenrock, "Direct self-control of inverter-fed machine," *IEEE Trans. Power Electron.*, Vol. 3, pp. 420-429, Oct. 1988.

[2] I. Takahashi and T. Naguchi, "A new quick-response and high efficiency control strategy of an induction motor," *IEEE Trans. Ind. Applicat.*, Vol. 1, pp. 820-827, Sept./Oct. 1986.

[3] L. Zhong, M. F. Rahman, W. Y. Hu, and K. W. Lim, "Analysis of direct torque control in permanent magnet synchronous motor drives," *IEEE Trans. Power Electron*., Vol. 12, pp. 528-536, May 1997.

[4] L. Zhong, M. F. Rahman, W. Y. Hu, and K. W. Lim, "A direct torque controlled interior permanent magnet synchronous motor drive incorporating field weakening," *IEEE Trans. Ind. Applicat.*, Vol. 34, pp. 1246-1253, Nov./Dec. 1998.

[5] L. Tang, L. Zhong, M. F. Rahman and Y. Hu, "A novel direct torque control for interior permanent magnet synchronous machine drive system with low ripple in flux and torque and fixed switching frequency," *IEEE Trans. Power Electron.*, Vol. 19, pp. 346-354, March 2004.

[6] L. Zhong, M. F. Rahman, W. Y. Hu, K. W. Lim and M. A. Rahman, "A direct torque controller for permanent magnet synchronous motor drives," *IEEE Trans. Energy Conv.*, Vol. 14, pp. 637-642, Sept. 1999.

[7] C. French and P. Acarnley, "Direct torque control of permanent magnet drives," *IEEE Trans Ind. Applicat.*, Vol. 1, pp. 1080-1088, Sept./Oct. 1996.

[8] C. Lascu, I. Boldea and F. Blaabjerg, "A modified direct torque control for induction motor sensorless drive," *IEEE Trans. Ind. Applicat.*, Vol. 36, pp.122-130, Jan./ Feb. 2000.

[9] M. F. Rahman, L. Zhong and K. W. Lim, "A direct torque controlled interior permanent magnet synchronous motor drive without a speed sensor," *IEEE Trans. Energy Conv.*, Vol. 18, pp. 17-22, March 2003.

[10] M. E. Haque, L. Zhong and M. F. Rahman, "A sensorless

initial rotor position estimation scheme for a direct torque controlled interior permanent magnet synchronous motor drive," *IEEE Trans. Power. Electron.*, Vol. 22, pp. 2487-2498, Nov. 2007.

[11] S. Bolognani, R. Oboe and M. Zigliotto, "Sensorless full digital PMSM drive with EKF estimation of speed and position," *IEEE Trans. Ind. Electron*., vol. 18, pp. 1376-1383, Nov. 2003.

[12] M. F Rahman., M. E. Haque, L. Tang, and L. Zhong, "Problems associated with the direct torque control of an interior permanent magnet synchronous motor drive and their remedies," *IEEE Trans. Ind. Electron*., Vol. 51, pp. 799-809, Aug. 2004.

[13] B. Nahid-Mobarakeh, F. Meibody-Tabar, and F.-M. Sargos, "Back EMF estimation-based sensorless control of PMSM: Robustness with respect to measurement errors and inverter irregularities," *IEEE Trans. Ind. Electron*., Vol. 43, pp. 485-494, March/April 2007.

[14] I. Boldea, C. I. Pitic, C. Lascu, G.-D. Andreescu, L. Tutelea, F. Blaabjerg and P. Sandholdt, "DTFC-SVM motion sensorless control of a PM-assisted reluctance synchronous machine as starter alternator for hybrid vehicles," *IEEE Trans. Power. Electron.*, Vol. 21, pp 711-719, May 2006.

[15] M. Corley and R.D. Lorenz, "Rotor position and velocity estimation for a salient-pole permanent magnet synchronous machine at standstill and high speeds," *IEEE Trans. Ind. Applicat.*, Vol. 43, pp 784-789, July/Aug. 1998.

[16] G.-D. Andreescu, C. I. Pitic, F. Blaabjerg and I. Boldea, "Combined flux observer with signal injection enhancement for wide speed range sensorless direct torque control of IPMSM drives," *IEEE Trans. Energy Conv*., Vol. 23, pp 393-402, June 2008.

[17] Z. Xu and M. F. Rahman, "Direct torque and flux regulation of an IPM synchronous motor drive using variable control approach," *IEEE Trans. Power. Electron*., Vol. 22, pp. 2487-2498, Nov. 2007.

[18] Z. Xu and M. F. Rahman, "An adaptive sliding stator flux observer for a direct torque controlled IPM synchronous motor drive," *IEEE Trans. Ind. Electron*., Vol. 54, pp. 2398-2406, Oct. 2007.

[19] M. Barut, S. Bogosyan and M. Gokasan, "Experimental Evaluation of Braided EKF for Sensorless Control of Induction Motors," *IEEE Trans Ind. Electron*., Vol. 55, No. 2, pp. 620-632, 2008.

[20] M. Barut, S. Bogosyan and M. Gokasan, "Speed sensorless estimation for induction motors using Extended Kalman Filters," *IEEE Trans. Ind. Electron*., Vol. 54, pp. 272-280, Feb. 2007.

[21] Y.S. Jeong, R. D. Lorenz, T. M. Jahns and S.K. Sul, "Initial rotor position estimation of an interior permanent magnet synchronous machine using carrier-frequency injection methods," *IEEE Trans. Ind. Applicat.*, Vol. 41, pp. 38-45, Jan./Feb. 2005.

[22] A. Piippo, M. Hinkkanen and J. Luomi, "Signal injection in sensorless PMSM drives equipped with inverter output filter," *IEEE Trans. Ind. Applicat.*, Vol.44, pp. 1614-1620, Sept./Oct. 2008.

[23] C. Caruana, G.M. Asher, K.J. Bradley and M. S. Woolfson, "Flux position estimation in cage induction machines using synchronous injection and Kalman filtering," *IEEE Trans. Ind. Applicat*., Vol. 39, pp 1372-1378, Sept./Oct. 2003.

[24] D. Cascadei, G. Serra, A. Stefani, A. Tani and L. Zarri, "DTC drives for wide speed range applications using a robust flux weakening algorithm," *IEEE Trans. Ind. Electron*., Vol. 54, pp.2451-2461, Oct. 2007.

[25] S. Sayeef and M. F. Rahman, "Improved low speed performance of a PI-DTC interior PM machine with compensations of dead-time effects and forward voltage drops," *in proc. of Conf. Rec. of International Conference on Power Electronics*, pp.906-911, 2007.

Gilbert Foo received his Diploma in Electrical and Electronics Engineering with Distinction from Inti College, Malaysia in 2004. He received a Bachelor of Electrical Engineering degree with First Class Honors from the University of New South Wales, Sydney, Australia in 2007. He is currently pursuing his PhD at the University of New South Wales, Sydney, Australia. His research interests are in electrical machines and drives.

M. F. Rahman received his Bachelor of Electrical Engineering degree with First Class Honors from the Bangladesh University of Engineering and Technology, Dhaka in 1972. He received a Masters of Engineering degree and his PhD from the University of Manchester Institute of Science and Technology, U. K. in 1975 and 1978 respectively. He subsequently worked as a System Design Engineer for General Electric, U. K., Rugby for two years before joining the National University of Singapore in 1980. He joined the University of New South Wales, Sydney, Australia in 1988 as a Senior Lecturer where he is currently a full Professor. His research interests are in electrical machines, drives and power electronics.